Supporting Information

Selective Electroreduction of CO_2 to Ethanol over Highly Stabile Catalyst Derived from Polyaniline/$CuBi_2O_4$

Yong Yang[a], Anbang He[a], Ming Yang[a], Qian Zou[a], Hui Li[a], Zuohua Liu[ab], Changyuan Tao*[ab] and Jun Du*[ab]

(a:College of Chemistry and Chemical Engineering, Chongqing University, Chongqing 401331, China

b: State key laboratory of coal mine disaster dynamics and control, Chongqing University, 174 Shazheng Street, Shapingba, Chongqing, China.*)*

1. Experimental Section

1.1 Materials and methods

1.1.1 Chemical Materials: Copper acetate monohydrate ($C_4H_6CuO_4 \cdot H_2O$, AR), Potassium hydroxide (KOH, AR), Bismuth nitrate pentahydrate ($Bi(NO_3)_3 \cdot 5H_2O$, AR), Potassium bicarbonate ($KHCO_3$, AR), Ammonium persulfate ($(NH_4)_2S_2O_8$ or APS, AR), polyvinyl pyrrolidone K30 (PVP, AR) was purchased from Chron-Chemicals (Chengdu, China) and used as received; aniline (C_6H_7N, AR) was purchased from Sigma-Aldrich and used after decompress distillation.

1.1.2 Synthesis of Cu_2O

Cu_2O was synthesized by a method reported in literature[1], for typical procedure: 5.0 mL NaOH aqueous solution (2.0 M) carefully dropped into 50 mL $CuCl_2$ aqueous solution (0.01 M) at 55°C. After adequately stirring for 0.5 h, 5.0 ml ascorbic acid aqueous solution (0.6 M) slowly drop into the solution. The mixed solution was continuously stirred at 55°C for 3 h. The product was collected by centrifugation and decanting, then cleaned with distilled water, and finally dried in vacuum at 80°C for 12 h.

1.1.3 Synthesis of $CuBi_2O_4$

$CuBi_2O_4$ was synthesized by improved hydrothermal method[2]. As a typical procedure, 181.9 mg $Bi(NO_3)_3 \cdot 5H_2O$ completely dissolved in 20 mL HNO_3 aqueous solutions (2.0 vol.%), then

PVP (0.75 g) was added into the solution under continuously ultrasound to form solution A. 37.5 mg $Cu(CH_3COO)_2 \cdot H_2O$ fully dissolved in 20 mL deionized, and dropped into solution A. Then, 20 mL KOH (2.0 M) was added dropwise into the mixture and kept continuously stirring for 0.5 h at room temperature. The solution mixture turned into a 100 mL Teflon-lined stainless-steel autoclave and sealed at 150 °C under autogenous pressure for 12 h. The mixture washed with deionized water multiple times after cooling to room temperature, finally vacuum dry at 80°C for 12 h.

1.1.4 Synthesis of PANi/$CuBi_2O_4$

PANi/$CuBi_2O_4$ was synthesized by in-situ polymerized growth method. Typically, 12.0 mg fresh aniline which had done the decompress distillation at 150°C, dissolved completely 20 mL aqueous ethanol solution (25 vol.%). Then, 80 mg $CuBi_2O_4$ were dispersed in the solution and kept adequately stirring for 5 h to form the high-spread mixture, meanwhile 23.45 mg APS dissolved in 20 mL hydrochloric acid (0.2 vol.%) and was added dropwise into the mixture carefully. Specifically, the polyreaction need react at room temperature for 30 min and quickly transfer to ice bath (0~5°C) for 24 h. Subsequently, the product washed at least 5 times with ultrapure water, and vacuum dry at 80°C for 24 h.

1.1.5 Synthesis of $CuBi_2O_4$-CR

$CuBi_2O_4$-CR was synthesized by H_2 reduction method. 0.1 g $CuBi_2O_4$ which synthesized in aforementioned work, was pretreat at N_2 (30 mL/min,99.99%) at 200°C for 2 h, then, reduced in the H_2 atmosphere (10 mL/min,99.999%) at 500°C for 3 h. Subsequently, cooled to the room temperature and obtained the material.

1.1.6 Synthesis of Bi_2O_3

Bi_2O_3 was synthesized by hydrothermal method. Typically, 2.0 mmol $Bi(NO_3)_3 \cdot 5H_2O$ and 3.0 mmol structural inducers dissolved on 40 mL deionized water, and kept adequately stirring for 45 min. Then, 40 mL alkali liquor (0.45 mM) added to the above solution, and kept continuous stirring for 2 h. Subsequently, the solution mixture turned into a 100 mL Teflon-lined stainless-steel autoclave and sealed at 150 °C under autogenous pressure for 12 h. The mixture washed deionized water multiple times after cooling to room temperature, finally vacuum dry at 80°C for 12 h. The formulations of different lye and structural inducers are shown in the Table-S 1.

Table S1. Three Bi_2O_3 was synthesized by different structure inducers and lye environments

Designation	Alkaline	Structural inducers
A	NaOH	Na_2SO_4
B	Urea	Ethane diamine
C	Urea	Glycol

1.2 Materials characterizations.

The crystal structures were investigated by XRD apparatus using a Rigaku D/max-3C, equipped with a graphite monochromator for Cu Kα (40 kV, 40 mA, λ=1.542 Å) radiation. The SEM and TEM characterizations were carried out using an JSM-7800F and FEI Talos F200s G2, equipped with energy dispersive X-ray spectroscopy (EDX). X-ray photoelectron spectroscopy (XPS) study was performed on the Kratos AXIS Ultra DLD instrument with monochromatic A1 Kα X-ray source (1486.6 eV) at power of 450 W (30 mA, 15kV). The TGA was performed using a TGA-DSC1 1600LF, and the analysis was carried out in N_2 with the heating rate was 5^{o}C min^{-1}。

CO_2-TPD and CO-TPD: TPD was carried out on TP-5080. **For CO_2-TPD**, the sample was reduced under H_2 at 100^{o}C first and then cooled down to room temperature in Ar.[3] The sample immersion CO_2-flowing (99.99%) atmosphere (10 mL/min) for 1h at 200^{o}C to achieved highest adsorption. Then, 35 mL/min He gas (99.99%) was passed through to remove the physical adsorptive CO_2 on 300^{o}C for 30 min. The test process was carried out temperature program of desorption with heat rate of 5^{o}C/min from 100^{o}C~600^{o}C. **For CO-TPD**, the samples pretreated at 100^{o}C. CO (99.99%) passed through the sample with flow-rate 10 mL/min at 50^{o}C for 1 h. 35 mL/min He gas (99.99%) was passed through to remove the physical adsorptive CO on 100^{o}C for 30 min. The test was run at a heat rate of 5^{o}C/min.

2. Electrochemical Measurement

2.1 Preparation of electrodes

To make the work electrode, 4.2 mg catalyst dispersed in a mixture contained 395 μL isopropanol and 5 μL Nafion ionomer solution (5 wt% in H_2O) by continuously sonicate for 15 min. Then, 5 μL of the catalyst slurry (contained 0.05 mg) uniformly coated on glassy carbon electrode (0.07 cm^{-2}). Pt (99.99%) worked as the counter electrode, while the saturated calomel electrode (SCE) as the reference electrode.

2.2 The electro-chemical activation process

The Cyclic-Voltammetry process was used as the method of electrochemical activation for the electrode material which coated on the glassy carbon on CO_2 atmosphere. During the process of activation, the CV program was carried out until the curves no more change.

2.3 Electrochemical research

All electrochemical studies were carried out in a gastight H-cell which separated by Nafion-117 membrane. All the electrochemical experiments tested by electrochemical workstation and (CHI 760E, Shanghai CH Instruments Co., China) a typical three-electrode system. Before each test, a continuous ventilation had been done by high-purity N_2 (99.99%) to exclude any dissolved gases. Then the pure CO_2 (99.99%, 6 mL/min) bubbled into electrolyte for at least 30 min to saturate the 0.1 M $KHCO_3$ (298 K).

2.4 EIS test

The EIS measurement was carried out in 0.1 M $KHCO_3$ solution at -1.0 V with amplitude of 5 mV of 1 to 10^5 Hz in different atmosphere.

2.5 Double-layer capacitance (C_{dl}) tests

The electrochemically active area is positive relevant to with C_{dl} value, which could determine by measuring the capacitance current related to double-layer charging and determining its dependence on the scan rate of the cyclic voltammogram (CV). The test carried out range from 0 V~0.1 V vs.RHE. The Δj was calculated by $\Delta j = j_a - j_c$ (j_a: anodic current density ; j_c : cathodic current density) at -0.05 V vs.RHE. The scan rates were 20, 30, 50, 80,100 and 120 mV s^{-1}.[4]

For better to compare with literature, all potential in this paper was rescaled to RHE reference:

$$E\ (vs.\ RHE) = E\ (vs.\ SCE) + 0.0591 \times pH + 0.24\ V$$

CO_2RR was conducted in CO_2-saturated 0.1 M $KHCO_3$ (298 K, pH=6.8) at room temperature and atmospheric pressure.

3. Product analysis.

3.1 Gas products analysis

The gaseous products produced in the electrocatalytic reduction process were collected by the gas bags and analyzed by gas chromatography (GC-1100), which was equipped with TCD detectors using N_2 as the carrier gas for H_2 and CO detection, meanwhile, it equipped with FID detectors using N_2 as the carrier gas for hydrocarbon gas detection. Due to the small difference in thermal conductivity between N_2 (5.8 cal/(cm·℃·s)) and CO (5.6 cal/(cm·℃·s)), therefore, the use of TCD

detection will bring greater error. Hence, we used CO gas analyzer (Sensonic 4000) for more precise measurement.

The calculations of Faradaic efficiencies (FE) of gaseous products by followed equation:

$$FE = \frac{n_{gas}}{Q/zF} \times 100\%$$

n_{gas} : moles of gas product (mol);

Q: electric quantity (C);

F: Faradaic constant (96485 C/mol)

z: the number of electrons for generate the gas product

3.2 Liquid products analysis

The liquid product was analyzed by ^{1}H NMR (Agilent DD2, 600M MHz) in deuteroxide. Typically, add 0.8 μL of DMSO (as the internal standard substance) into 20 mL of electrolyzed electrolyte, and ultrasound for 0.5 h to mix well. Subsequently, 400 μL of the mixed solution and 110 μL of D_2O (as a deuterated reagent) were added to the NMR tube, let it stand overnight to deuterate completely. Then 600 M ^{1}H NMR was used for analysis, and the excitation sculpting was used to effectively suppress the water peak. (Figure S10)

The FE of liquid products is:

$$FE = \frac{n_{liquid}}{Q/zF} \times 100\%$$

n_{liquid} : moles of liquid product (mol);

Q: electric quantity (C);

F: Faradaic constant (96485 C/mol)

z: the number of electrons for generate the gas product

4. Computational Method

All calculations were performed by using the DMol^3 package.[5, 6] The DFT semi-core pseudopotential (DSSP) method was employed to treat core electrons, which introduced some degree of relativistic correction into the core. The gradient-corrected functionals (GGA) with the Perdew, Burke, and Ernzerhof (PBE) functional were adopted to describe the exchange and correlation potential,[7] meanwhile, Grimme's scheme[8] was used to deal with the dispersion correction for DFT. The double numerical plus polarization (DNP) was chosen as the atomic orbital basis set. The surface of catalyst was described by a simplified model system. For the

surface of Cu, a periodic (6×5) Cu (100) with five-layer slabs, while for the surface of Cu-Bi, doped Bi atoms on the above surface of Cu, separated perpendicularly by 20 Å vacuum in the z-direction. To ensure high-quality computational results, the convergence tolerances of energy, maximum force, and displacement were set to 1.0×10^{-5} Ha, 0.002 Ha·Å^{-1}, 0.005 Å, respectively, and the global orbital cut-off was set with fine quality scheme. The reciprocal space was sampled using a 5 × 5 × 1 k-point grid for the geometry optimizations with the atoms on the two top layers relaxation, while a 10×10×1 grid was used for the electronic structure computations. The charge transfer and the magnetic moment were determined according to the Hirshfeld method.[9] The most favorable adsorption structure was explored for all of the intermediate species.

The adsorption energies (E_{ads}) were calculated according to the following equation:[9]

$$E_{ads} = E_{adsorbate/substrate} - E_{adsorbate} - E_{substrate}$$

$E_{adsorbate/substrate}$: the total energy of the adsorbate-substrate system in the equilibrium state. $E_{adsorbate}$ and $E_{substrate}$: the total energy of the free adsorbate and substrate, including hydrocarbon, metal-oxide cluster and H atom, respectively.

The computational hydrogen electrode (CHE) model[10] was used to calculate the free energies of CO_2 reduction intermediates via the following equation:

$$\Delta G = \Delta E + \Delta ZPE - T\Delta S + \int c_p dT$$

where ΔE is the electronic adsorption energy, ΔZPE is the variation in zero-point energy (ZPE) and ΔS is the change in entropy before and after the reaction. T is the temperature (298 K). The standard entropy values were cited from the literature. [4]Furthermore, the free energy calculated via DFT can be extrapolated to other potentials by following equation:[9-11]

$$\Delta G_{act} = \Delta G^0(U^0 = 0) + n\beta(U - U^0)$$

where β is the reaction effective symmetry factor and was approximated to be 0.5 for all steps; while the n was the amount of electron transferred and single electron transmission for all steps.

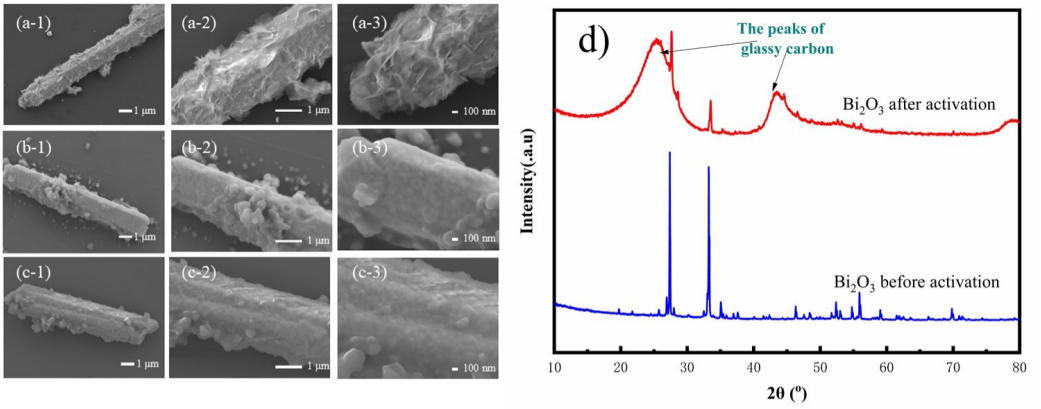

Figure S1. The SEM of catalyst: a) Bi_2O_3; b) Bi_2O_3@PANi; c) Bi_2O_3@PANi after activation; d) Bi_2O_3@PANi before and after CV activation.

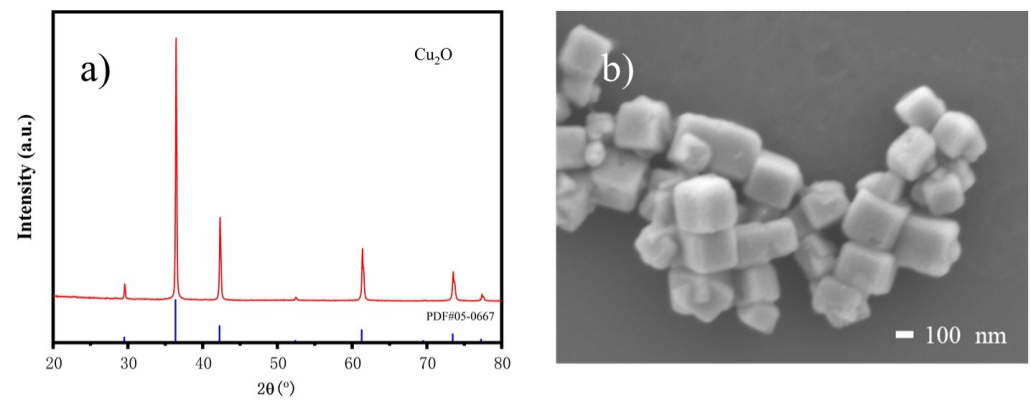

Figure S2. a) XRD and b) SEM of Cu_2O

Table S2. The contents of the series of $CuO\text{-}CuBi_2O_4$-x

Sample	Inventory Rating (mg)		Quantitative analysis（%）		
	$Bi(NO_3)_3 \cdot 5H_2O$	$Cu(Ac)_2$	$CuBi_2O_4$	CuO	Bi_2O_3
$CuO\text{-}CuBi_2O_4$-A	181.9	18.8	64.8	~	35.2
$CuO\text{-}CuBi_2O_4$-B	181.9	37.5	100	~	~
$CuO\text{-}CuBi_2O_4$-C	181.9	56.3	96.3	3.7	~
$CuO\text{-}CuBi_2O_4$-D	181.9	75.0	91.6	8.4	~
$CuO\text{-}CuBi_2O_4$-E	181.9	112.5	84.1	15.9	~
$CuO\text{-}CuBi_2O_4$-F	181.9	150.0	60.5	39.5	~

“~”： the content bellowed detection limit of XRD and no relevant peak signal was detected

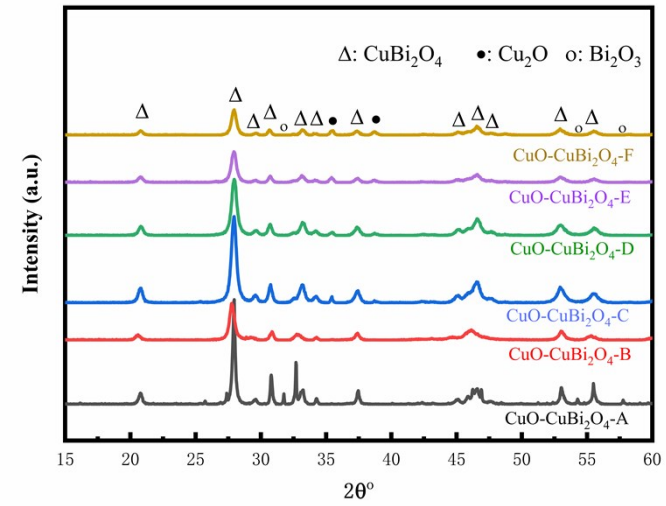

Figure S3. XRD patterns for the series of $CuO\text{-}CuBi_2O_4$-x

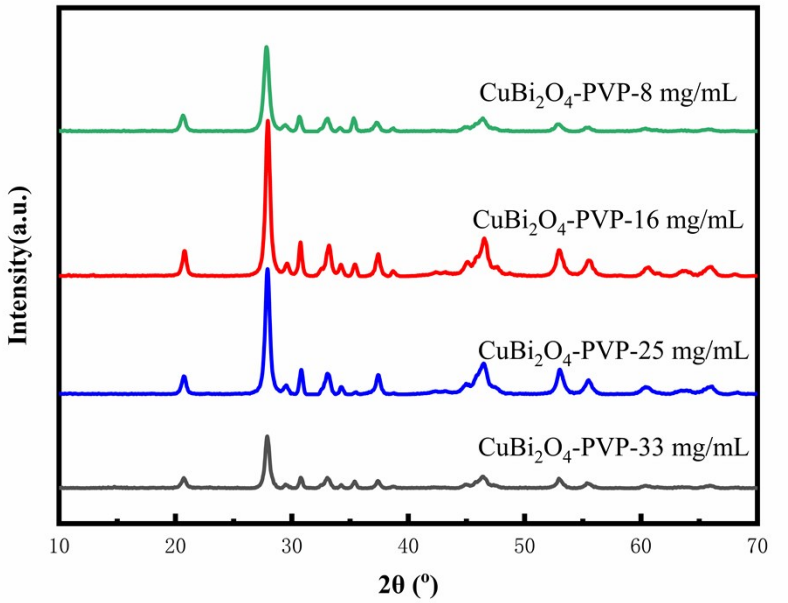

Figure S4. The optimization for the concentration of structure inducer PVP

As above figure shows, when the PVP concentration is 16 mg/mL, $CuBi_2O_4$ has the best $CuBi_2O_4$ crystallinity.

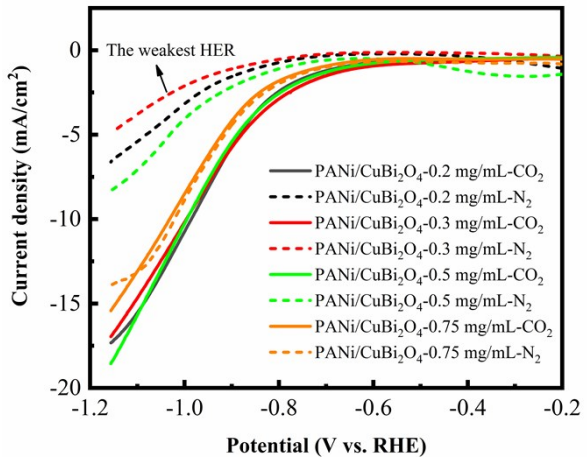

Figure S5. LSV curves of PANi/$CuBi_2O_4$ synthesized in different aniline concentration

By comparing the current density difference between N_2 atmosphere and CO_2 atmosphere, the synthesized catalyst has the highest CO_2 activity when the aniline concentration is 0.3 mg/mL

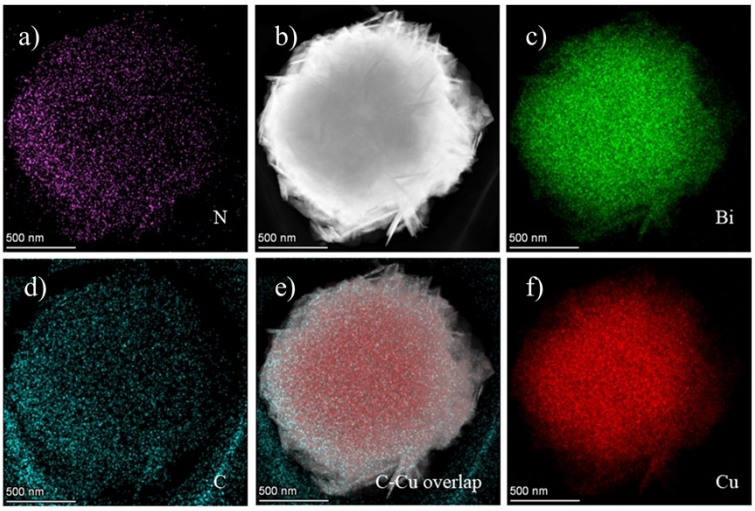

Figure S6. The images of b) STEM and mappings for the surface laminated structure of PANi/$CuBi_2O_4$; a) N; c) Bi; d) C; e) C-Cu overlap; f) Cu.

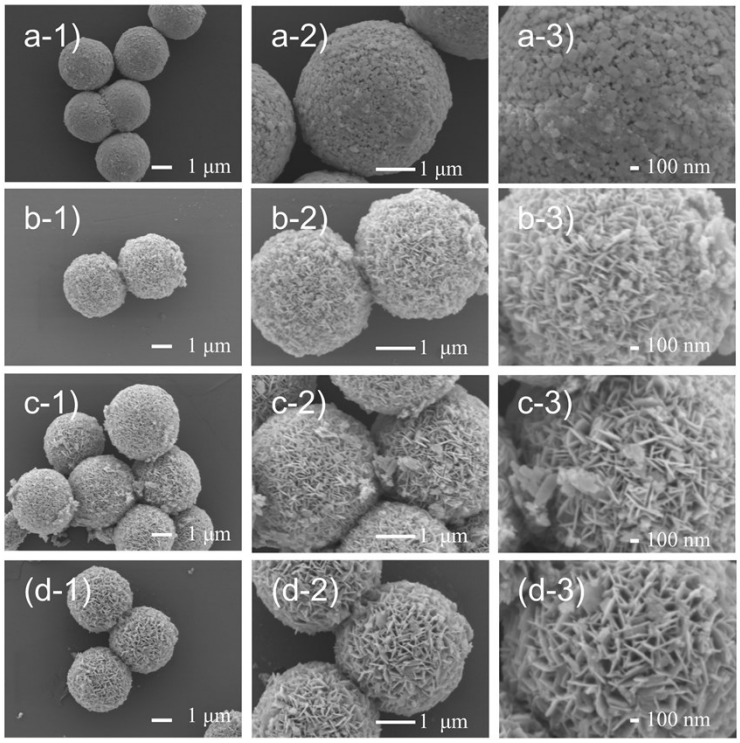

Figure S7. The SEM images of $CuBi_2O_4$: a-1~3) before acid etching; b-1~3) etching by 0.1 vol.% hydrochloric acid, c-1~3) etching by 0.2 vol.% hydrochloric acid, d-1~3) etching by 0.3 vol.%. hydrochloric acid

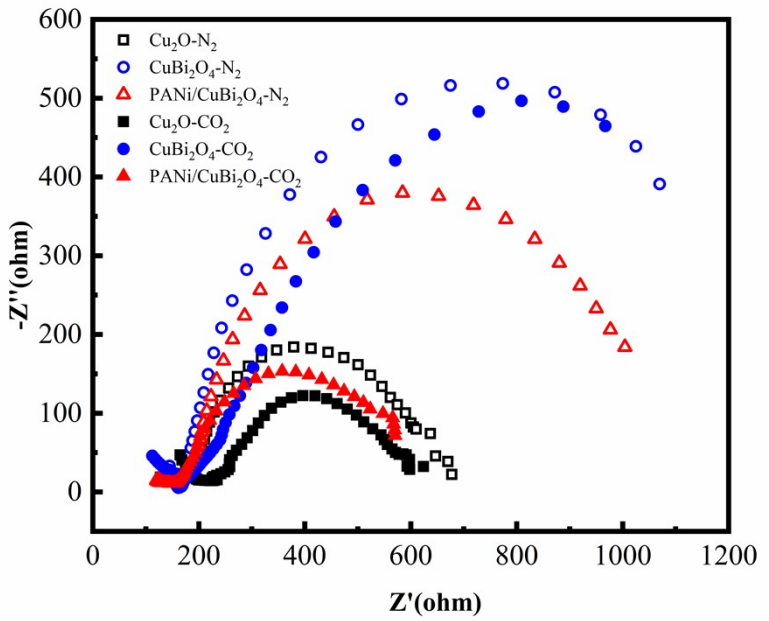

Figure S8. The EIS of three catalysts on the atmosphere of N_2 (Hollow tag) and CO_2 (Solid tag) at -0.96V vs RHE.

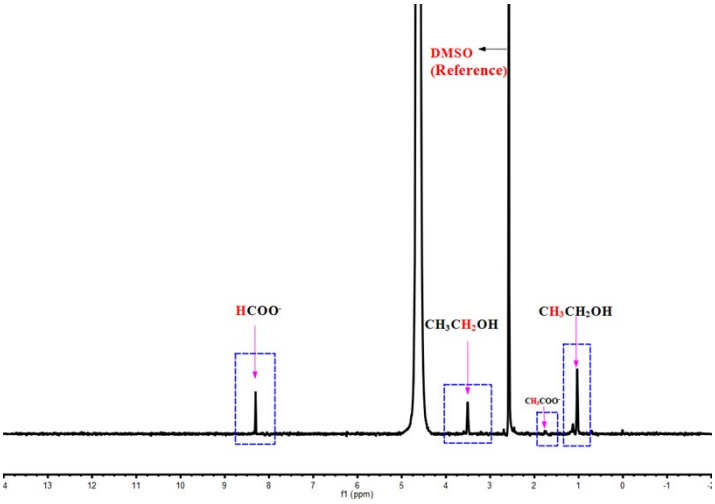

Figure S9. ^{1}H-NMR spectra of the liquid products of PANi/$CuBi_2O_4$ for CO_2RR at -0.96V vs RHE

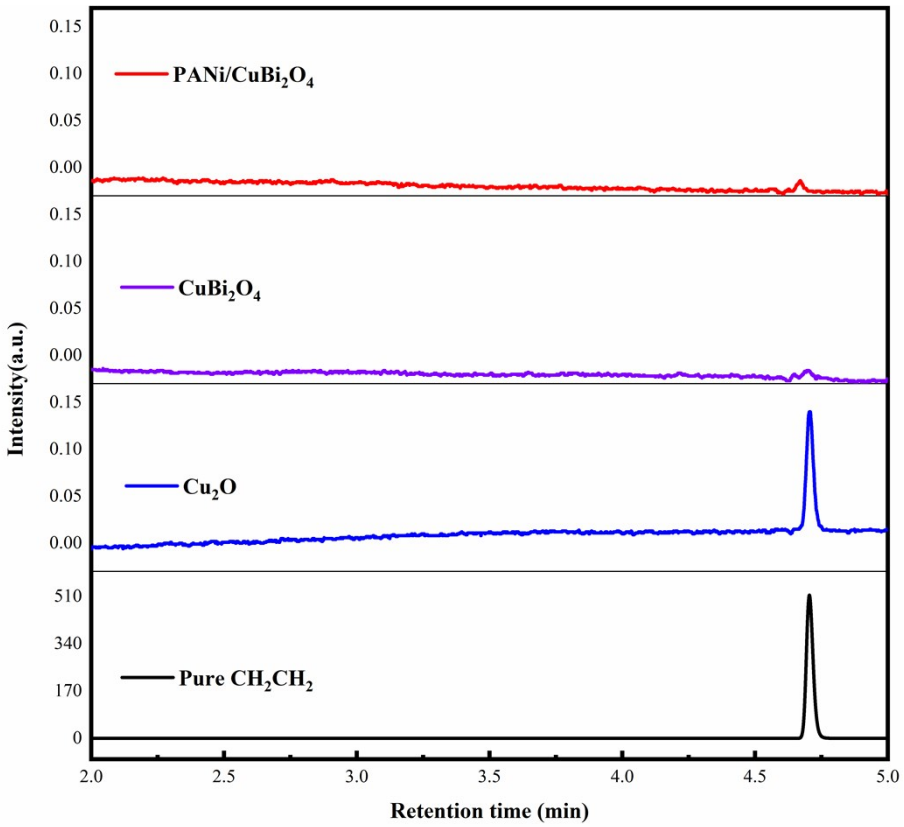

Figure S10. GC analysis of the C_2H_4 gas products by FID detector over different catalysts at -0.96V vs RHE

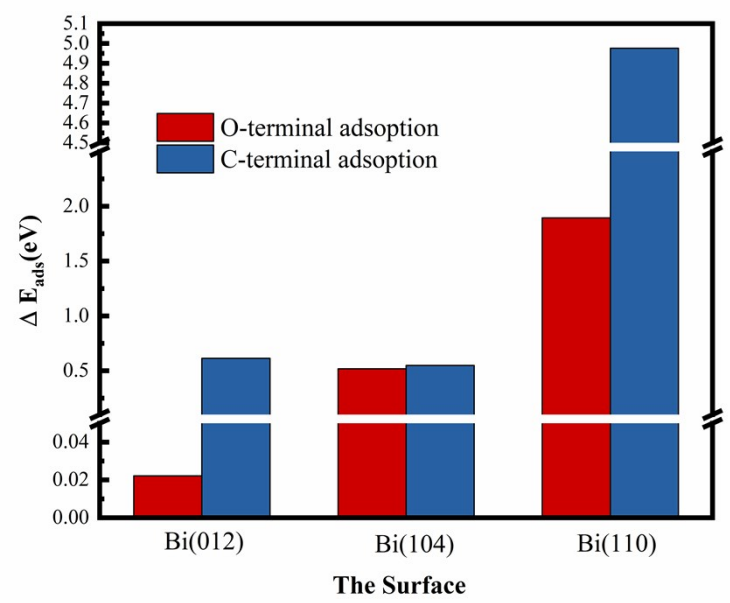

Figure S11. The ΔEads of CO_2 on lattice plane of Bi(012), (104), (110);

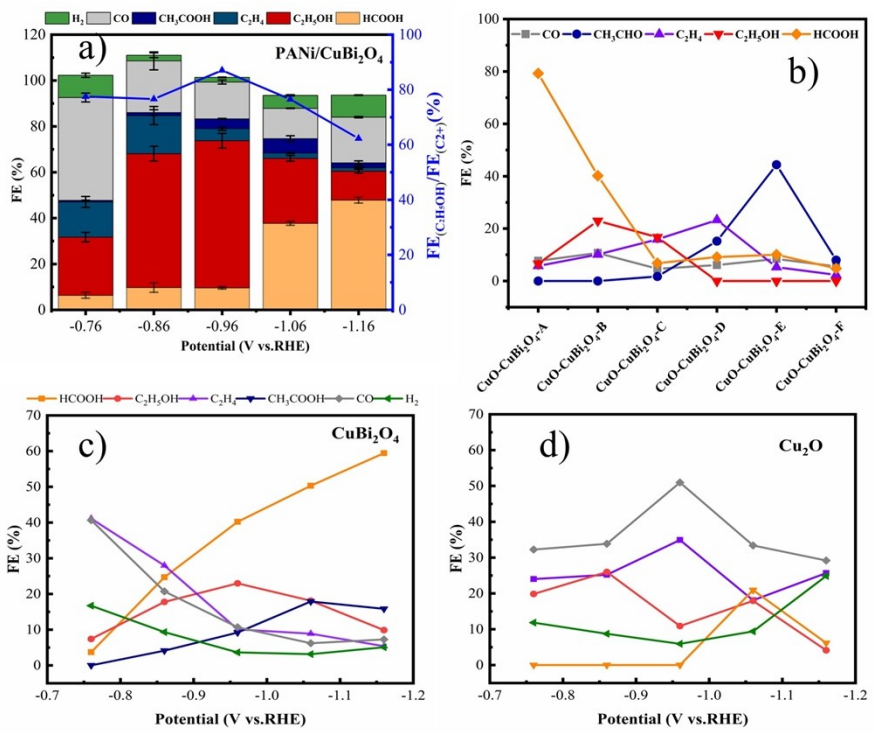

Figure S12. a) The CO_2RR products distribution over $PANi/CuBi_2O_4$ at different reaction potential; b) the FE analysis for different consistence of CuO and $CuBi_2O_4$ at -0.96 V vs. RHE.; The tendency of FE for catalysts: c) $CuBi_2O_4$, d) Cu_2O.

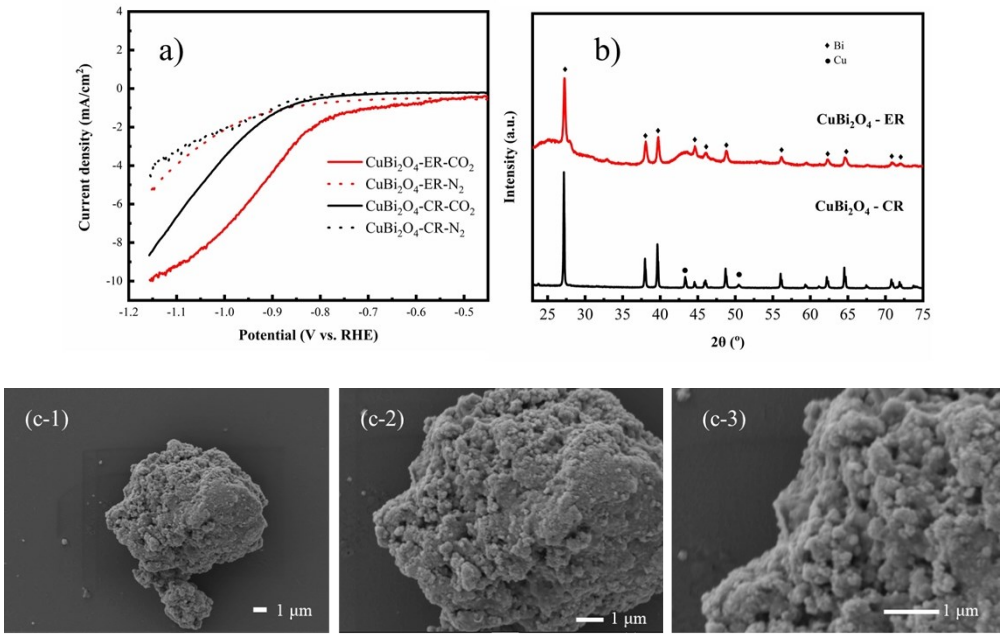

Figure S13. a) The LSV tests of catalysts in different atmosphere; b) XRD of the catalysts after reduction: $CuBi_2O_4$-ER (red line), $CuBi_2O_4$-CR (dark line); c-1~3) The SEM of $CuBi_2O_4$ after H_2 treatment in high temperature at different resolutions.

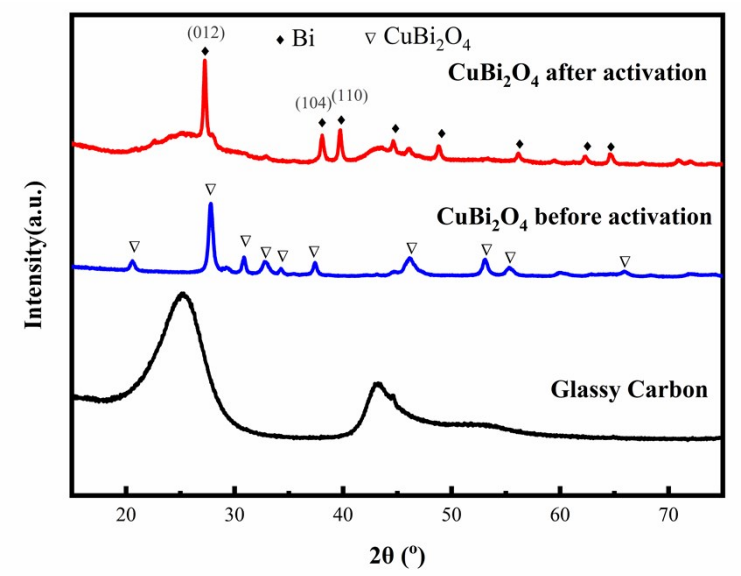

Figure S14. The XRD patterns of $CuBi_2O_4$ before and after CV activation

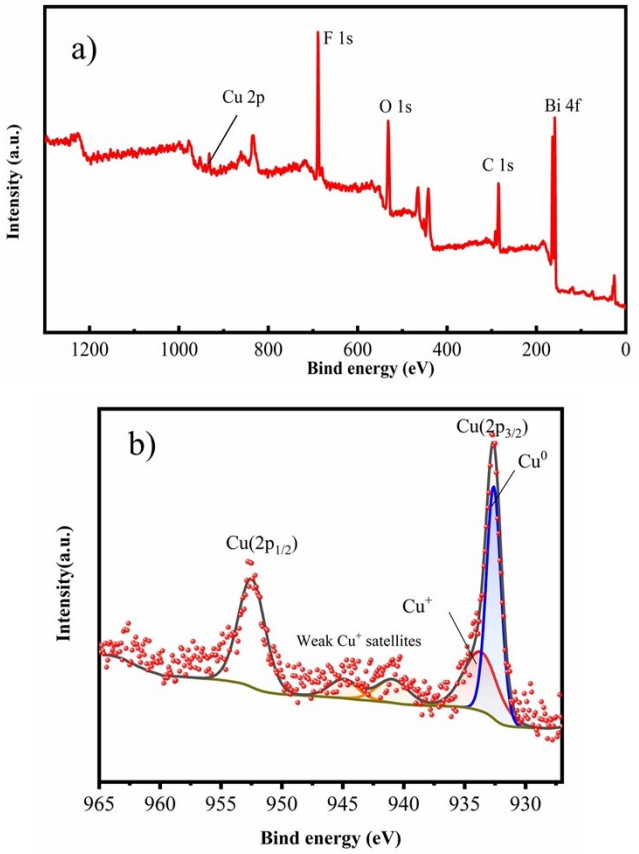

Figure S15. The XPS spectrum of $CuBi_2O_4$ after electrochemical activation: (a) survey XPS spectrum, (b) high-resolution Cu 2p XPS spectrum

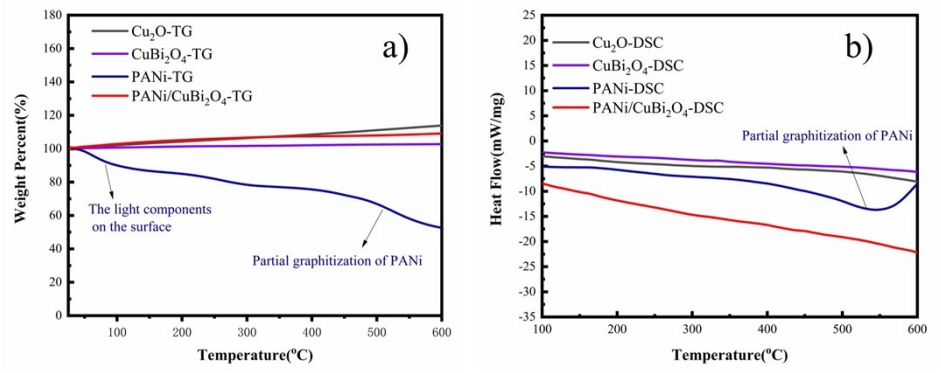

Figure S16. a) TG plots of catalysts; b) DSC plots of catalysts.

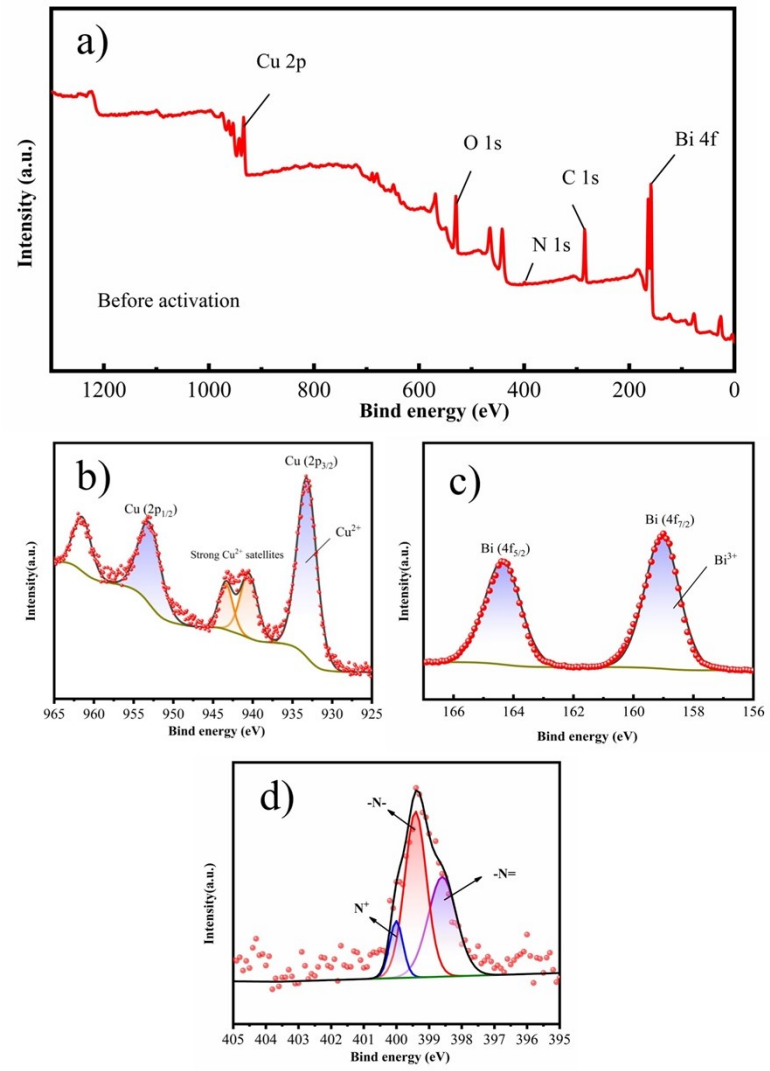

Figure S17. The XPS spectrum of PANi/$CuBi_2O_4$ before electrochemical activation: (a) survey XPS spectrum, (b) high-resolution Cu 2p XPS spectrum, (c) high-resolution Bi 4f spectrum, (d) high-resolution N 1s spectrum

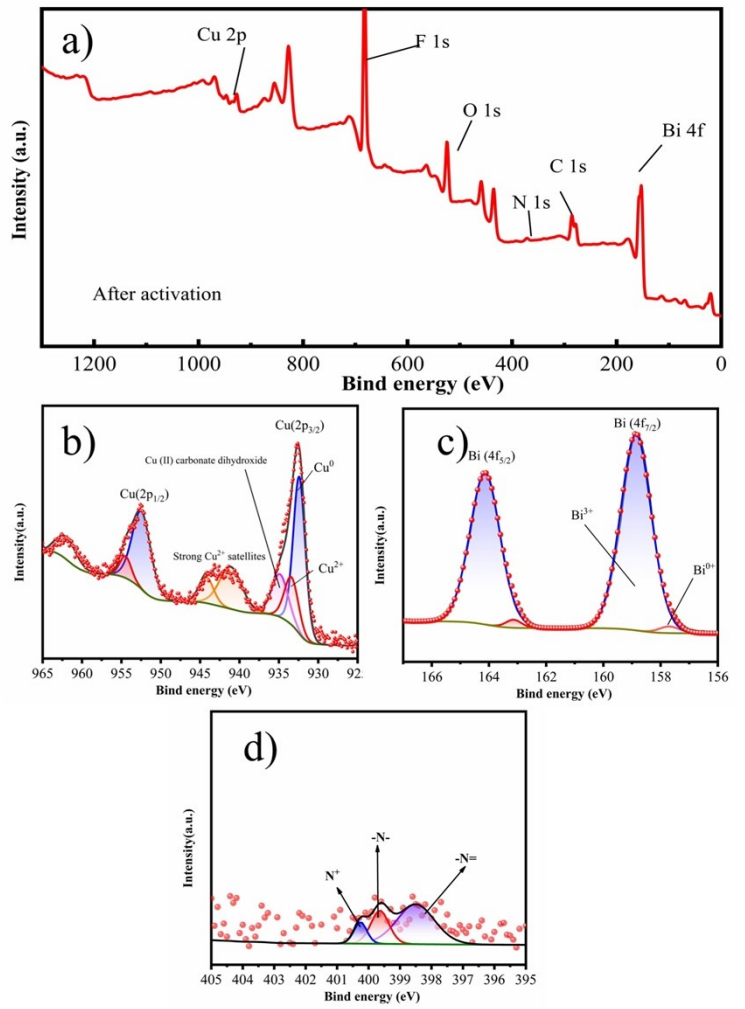

Figure S18. The XPS spectrum of PANi/$CuBi_2O_4$ after electrochemical activation: (a) survey XPS spectrum, (b) high-resolution Cu 2p XPS spectrum, (c) high-resolution Bi 4f spectrum, (d) high-resolution N 1s spectrum

Table S3. The surface content of Cu and Bi before and after the electrochemical activation

	Cu 2p (%)		**Bi 4f (%)**	
	Cu^{2+} / (Cu^{0+} +Cu^{2+})	Cu^{0+} / (Cu^{0+} +Cu^{2+})	Bi^{3+} / (Bi^{0+} +Bi^{3+})	Bi^{0+} / (Bi^{0+} +Bi^{3+})
Before activation	100	~	100	~
After activation	26.05	73.95	93.40	6.60

According to the XPS test results, after activation, the ratio of the sum of Cu atoms on the surface to the sum of Bi atoms was still 1:2. So the ratios of Cu^{0+} to Bi^{3+} was 5.6 to 1.

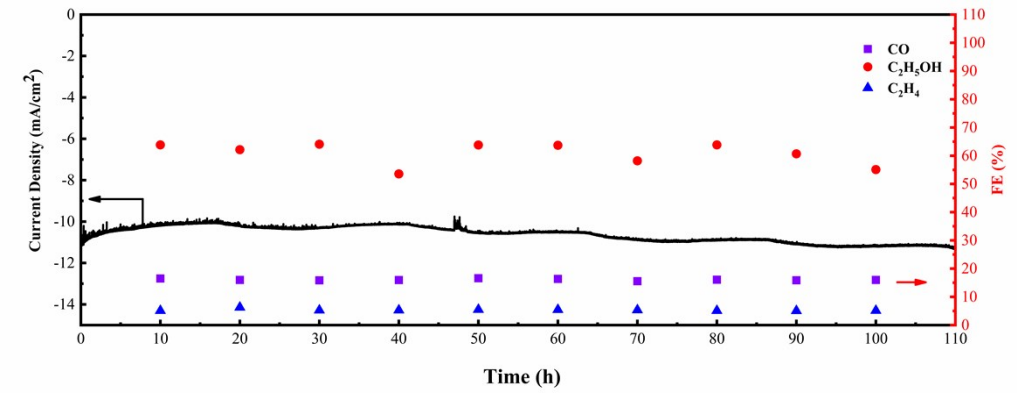

Figure S19. The long period stability test of PANi/$CuBi_2O_4$ with 110 h on -0.96 V vs RHE.

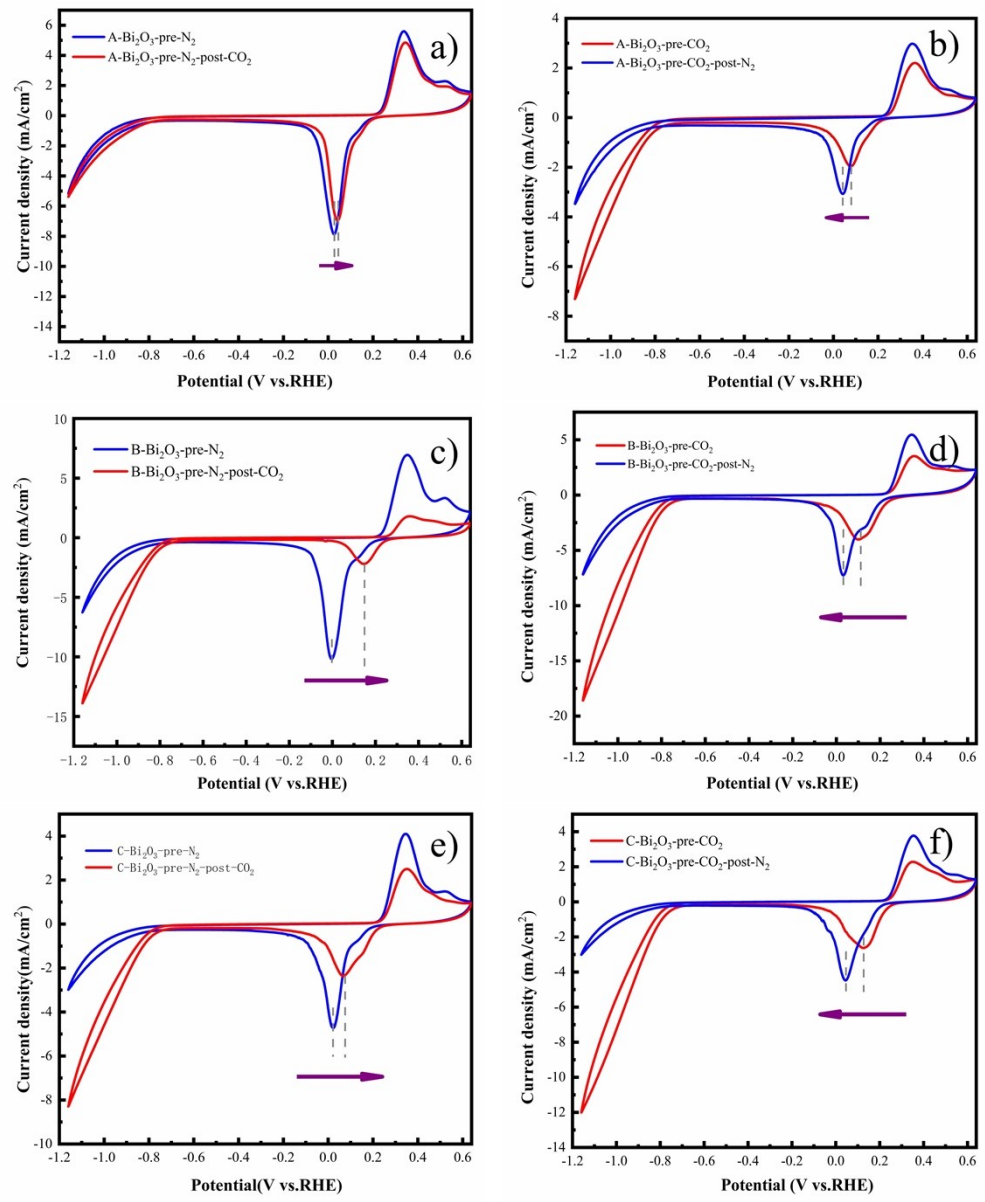

Figure S20. CV curves had been studied under different switching sequences of N_2 and CO_2 atmospheres for three Bi_2O_3.

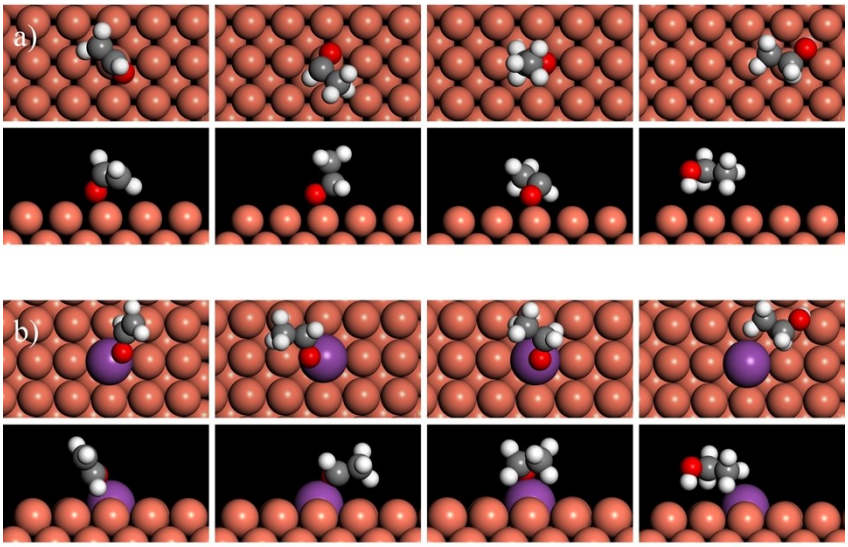

Figure S21. Proposed detail reaction steps for C_2H_3O* to C_2H_5OH: a) on the surface of Cu(100); and b) on the surface of Bi doped Cu(100).The atoms in yellow, violet, red, gray and white represent Cu, Bi, O, C and H, respectively.

The proposed reaction mechanism about C_2H_3O* to C_2H_5OH[4]

$$C_2H_3O^* + (H^+ + e^-) \rightarrow C_2H_4O^*$$

$$C_2H_4O^* + (H^+ + e^-) \rightarrow C_2H_5O^*$$

$$C_2H_5O^* + (H^+ + e^-) \rightarrow C_2H_5OH$$

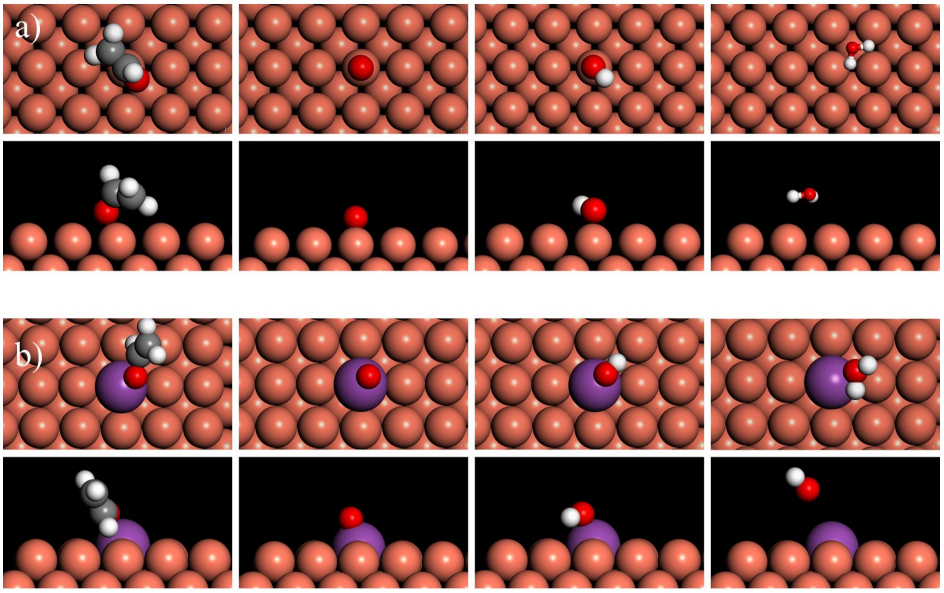

Figure S22. Proposed detail reaction steps for C_2H_3O* to C_2H_4: a) on the surface of Cu(100); and b) on the surface of Bi doped Cu(100). The atoms in yellow, violet, red, gray and white represent Cu, Bi, O, C and H, respectively.

The proposed reaction mechanism about C_2H_3O* to C_2H_4[4]

$$C_2H_3O^* + (H^+ + e^-) \rightarrow C_2H_4 + O^*$$

$$O^* + (H^+ + e^-) \rightarrow OH^*$$

$$OH^* + (H^+ + e^-) \rightarrow H_2O + *$$

Table S4. Comparison of alcohols in CO_2RR on various Cu-based catalysts.

	Catalyst	electrolyte	Reaction potential achieved highest FE of C_2H_5OH	$FE_{(C2+)}$	$FE_{(C2H5OH)}$	$FE_{(C2H5OH)}/FE_{(C2+)}$	Partial current density of ethanol (mA/cm^2)	Reference
(1)	$PANi/CuBi_2O_4$	0.1 M $KHCO_3$	-0.96 V vs RHE	73.64%	64.15%	87.05%	6.27 In H-Cell	This work
(2)	porous copper	0.1M $KHCO_3$	-1.1V vs RHE	78.00%	16.00%	20.51%	~31.2 In H-Cell	12
(3)	N-doped graphene quantum dots (NGQ) on CuO-derived Cu nanorods (NGQ/Cu-nr)	1.0 M KOH	-0.9 V vs. RHE	80.40%	52.40%	65.17%	147.8 In electrochemical flow cell	4
(4)	Planar Copper Nitride-Derived Mesoporous Copper（Cu_3N）	0.1 M $CsHCO_3$	-1.00 V vs RHE	68.00%	20.00%	29.41%	~3.56 gas-tight electrochemical cell	13
(5)	Cu GNC-VL	0.5 M $KHCO_3$	-0.87 V vs RHE	70.52%	70.52%	100 %	8.69 In H-Cell	14
(6)	$Ag\text{-}Cu_2O_{PB}$	0.1M $KHCO_3$	−1.2 V vs RHE	43.65%	34.15%	78.2%	~1.02 In H-Cell	15
(7)	Cu_4Zn	0.1 M $KHCO_3$	−1.05 V vs RHE	47.00%	29.1%	61.91%	~3.14 In H-Cell	16
(8)	BND	0.1M $NaHCO_3$	-1.0 V vs RHE	93.2%	93.2%	100%	~0.93 In H-Cell	17
(9)	Nitrogen-Doped Mesoporous Carbon	0.1 M $KHCO_3$	-0.56 V vs RHE	77%	77%	100%	~0.27 In H-Cell	18
(10)	Ag-G-NCF	0.1 M $KHCO_3$	-0.6 V vs RHE	85.2%	85.2%	100%	0.32 In H-Cell	19
(11)	Cu NPs	0.1 M $KHCO_3$	-0.5 V vs. RHE	76%	50%	65.79%	6.6 In H-Cell	20
(12)	$Ag_{0.14}/Cu_{0.86}$	1 M $KHCO_3$	−0.67 V vs.RHE	84%	41%	48.80%	250 In GDE	21

References:

1. T. C. W. H. Qing Hua, *Angew. Chem.* , 2014, **126**, 4956-4961.
2. Y. Zhang, G. Li, H. Zhao, F. Tian, S. Xiao and R. Chen, *CrystEngComm*, 2013, **15**.
3. W. Zheng, S. Nayak, W. Yuan, Z. Zeng, X. Hong, K. A. Vincent and S. C. Tsang, *Chem. Commun (Camb)*, 2016, **52**, 13901-13904.
4. C. Chen, X. Yan, S. Liu, Y. Wu, Q. Wan, X. Sun, Q. Zhu, H. Liu, J. Ma, L. Zheng, H. Wu and B. Han, *Angew. Chem. Int. Ed. Engl.*, 2020, **59**, 16459-16464.
5. Q. Zhang, S. Tao, J. Du, A. He, Y. Yang and C. Tao, *J. Mater. Chem. A*, 2020, **8**, 8410-8420.
6. Q. Zhang, A. He, Y. Yang, J. Du, Z. Liu and C. Tao, *J. Mater. Chem. A*, 2019, **7**, 24337-24346.
7. Z. Zhao and G. Lu, *ACS Catal.*, 2018, **8**, 3885-3894.
8. S. Grimme, *J. Comput. Chem.*, 2006, **27**, 1787-1799.
9. A. Seifitokaldani, C. M. Gabardo, T. Burdyny, C. T. Dinh, J. P. Edwards, M. G. Kibria, O. S. Bushuyev, S. O. Kelley, D. Sinton and E. H. Sargent, *J. Am. Chem. Soc.*, 2018, **140**, 3833-3837.
10. J. K. Nørskov, J. Rossmeisl, A. Logadottir and L. Lindqvist, *J. Phys. Chem. B,* 2004, **108**, 17886-17892.
11. X. Nie, M. R. Esopi, M. J. Janik and A. Asthagiri, *Angew. Chem. Int. Ed. Engl.*, 2013, **52**, 2459-2462.
12. C. Zou, C. Xi, D. Wu, J. Mao, M. Liu, H. Liu, C. Dong and X. W. Du, *Small*, 2019, **15**, e1902582.
13. M. Ebaid, K. Jiang, Z. Zhang, W. S. Drisdell, A. T. Bell and J. K. Cooper, *Chem. Mater.*, 2020, **32**, 3304-3311.
14. Y. Zhang, K. Li, M. Chen, J. Wang, J. Liu and Y. Zhang, *ACS Appl. Nano Mater.,* 2019, **3**, 257-263.
15. S. Lee, G. Park and J. Lee, *ACS Catal.*, 2017, **7**, 8594-8604.
16. D. Ren, B. S.-H. Ang and B. S. Yeo, *ACS Catal.*, 2016, **6**, 8239-8247.
17. Y. Liu, Y. Zhang, K. Cheng, X. Quan, X. Fan, Y. Su, S. Chen, H. Zhao, Y. Zhang, H. Yu and M. R. Hoffmann, *Angew. Chem. Int. Ed. Engl.*, 2017, **56**, 15607-15611.
18. Y. Song, W. Chen, C. Zhao, S. Li, W. Wei and Y. Sun, *Angew. Chem. Int. Ed. Engl.*, 2017, **56**, 10840-10844.
19. K. Lv, Y. Fan, Y. Zhu, Y. Yuan, J. Wang, Y. Zhu and Q. Zhang, *J. Mater. Chem. A*, 2018, **6**, 5025-5031.
20. D. Kim, C. S. Kley, Y. Li and P. Yang, *Proc. Nat. Acad. Sci.*, 2017, **114**, 10560-10565.
21. Y. C. Li, Z. Wang, T. Yuan, D. H. Nam, M. Luo, J. Wicks, B. Chen, J. Li, F. Li, F. P. G. de Arquer, Y. Wang, C. T. Dinh, O. Voznyy, D. Sinton and E. H. Sargent, *J. Am. Chem. Soc.*, 2019, **141**, 8584-8591.